Journal of Nuclear Materials 393 (2009) 522–526

Contents lists available at ScienceDirect

Journal of Nuclear Materials

journal homepage: www.elsevier.com/locate/jnucmat

Surface and bulk modification of W–La_2O_3 armor mock-up

F. Ghezzi [a,*], M. Zani [b], S. Magni [c], G.M. Vanacore [b], A. Tagliaferri [b]

[a] Istituto di Fisica del Plasma, University of Milano-Bicocca, 20125 Milan, Italy
[b] Dipartimento di Fisica, Politecnico di Milano, P.zza Leonardo da Vinci, 32-20133 Milan, Italy
[c] Department of Materials Science and Laboratory FIB/SEM 'Bombay', University of Milano-Bicocca, Via Cozzi 53, 20125 Milan, Italy

ARTICLE INFO

Article history:
Received 21 January 2009
Accepted 30 June 2009

ABSTRACT

W–(1%)La_2O_3 has been investigated after thermal exposure in the Quasi-Stationary Plasma Accelerator facility in order to obtain information regarding its surface damage and morphological modification. The profilometry measurements and the Scanning Electron Microscopy analysis showed that surface erosion and corrugation become more pronounced with increasing the thermal load. The La_2O_3 particle density inside the sample has been measured by Scanning Auger Microscopy. It decreases with increasing the thermal load and presents a negative gradient from the bulk to the surface.

1. Introduction

Metallic tungsten (W) is currently one of the candidate materials for the divertor of the International Thermonuclear Experimental Reactor (ITER) [1,2] thanks to its high thermal conductivity, low sputtering rate, its high melting point (T_{melt} = 3422 °C) and low vapor pressure (1.3×10^{-7} Pa at T_{melt}). However, due to its high Ductile-to-Brittle Transition Temperature (DBTT) (100–400 °C) and low machinability at room temperature (RT), the exploitation of pure W is difficult and expensive. Alloying W with other elements, such as Re and La, improves the above properties and reduces costs [3]. In particular, the addition of La_2O_3 to metallic tungsten improves the grain boundary strength at ambient and elevated temperatures, resulting in a remarkable increase of the thermal shock and creep resistance, and an improvement in the machinability and in high temperature tensile strength [4–6].

W–(1%)La_2O_3 has a higher recrystallization temperature as well as higher thermal strength than pure W [7], while maintaining a good machinability at room temperature with advantages in the total production costs. Moreover, W–La_2O_3 was selected as the reference high-Z armor for the divertor and baffle of ITER [8], due to the well balanced material properties, the expertise from other areas of application, lower costs for the machining with respect to W, as well as the moderate neutron fluence in the first generation to the ITER divertor. The drawbacks are a higher material price, an increased hardness (causing problems for hot-working), a lower thermal conductivity and a lack of knowledge on neutron irradiation damage. More details on W–La_2O_3 can be found in Ref. [3].

Thermal shock and creep resistance are of paramount importance during transient loads. While disruptions occur well above the W melting threshold (1 MJ/m^2) limiting the maximum allowable number of these events, Edge Localised Modes (ELMs) transients can occur below, at or just above the threshold. Since the ELM's transients are much more frequent than disruptions, it is important to know the surface damage and the morphological modification during these transients near the threshold. This work reports about surface and bulk microstructural modifications on a W–(1%)La_2O_3 divertor armor exposed in the Quasi-Stationary Plasma Accelerator (QSPA) facility.

2. Experiments

A W–La_2O_3 castellated armor was exposed to 100 ELM's transients at the QSPA facility, providing realistic heat loads (in terms of pulse duration and energy density) to simulate the expected ELMs and disruptions loads in ITER: details about the armor geometry, load distribution and the facility plasma parameters can be found in Refs. [9,10]. Here it is worth to remember that the plasma density was 10^{22} m^{-3}, the pulse duration was 500 μs, the maximum energy density was 1 MJ/m^2, located at the center of the target plate, and that the load had a Gaussian spatial distribution. The reference material was analyzed too and showed an average number density of 25×10^{-3}/μm^2 and an average size of 5×1 μm^2 in the section. Three samples sized 3×10 mm^2 were cut from the 10×10 mm^2 castellated tiles located at the center of the target along the transversal cross section: the samples, named A1, A2 and A3, received a series of repeated plasma pulses with an estimated energy density of 1, 0.8 and 0.6 MJ/m^2, respectively (see Fig. 1).

In order to evaluate the surface morphological changes and damages the samples have been analyzed with different

* Corresponding author. Tel.: +39 266173209; fax: +39 266173239.
E-mail address: ghezzi@ifp.cnr.it (F. Ghezzi).

0022-3115/$ - see front matter © 2009 Elsevier B.V. All rights reserved.
doi:10.1016/j.jnucmat.2009.06.031

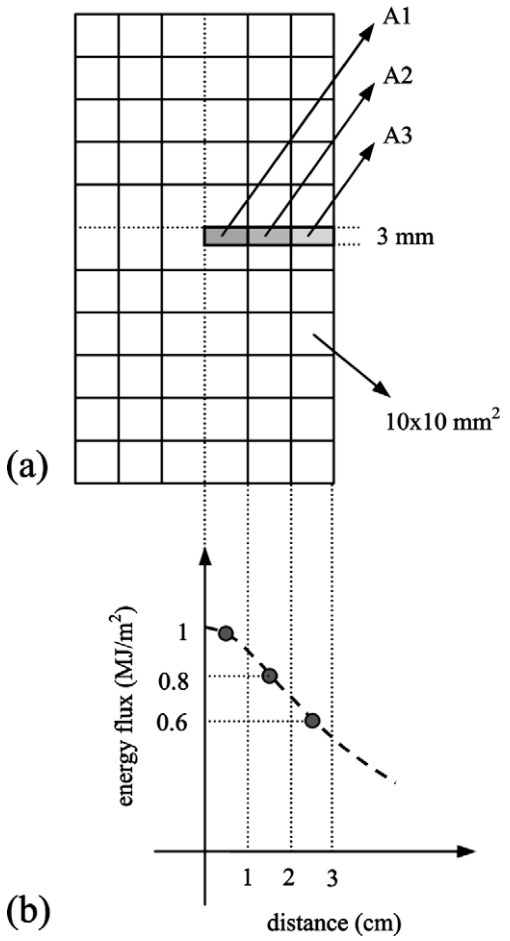

Fig. 1. (a) Top view layout of the target, continuous lines correspond to castellated sample and bold boxes to the three samples A1, A2 and A3 cut from the armor (b) cross section of energy density distribution of plasma pulse.

techniques: profilometry and optical microscopy at Istituto di Fisica del Plasma, Scanning Electron Microscopy (SEM) at the Laboratory FIB/SEM 'Bombay' of the University of Milano-Bicocca, Scanning Auger Microscopy (SAM) at Dipartimento di Fisica of the Politecnico di Milano.

3. Results

Fig. 2 shows the 3D profiles obtained with a mechanical profilometer for the three samples investigated. The samples appear corrugated with the crests parallel to the direction of the plasma flux.

The roughness and the average height of the crests are summarized in Table 1. The table reports the results relative to a W and Carbon–Fiber–Reinforced-Carbon (CFC) exposed to the same load for comparison [11].

Fig. 3 reports the SEM images of the sample surface. It should be noted that ordered viscous fingers form due to the melt motion induced by gravity (the sample surface was inclined at 30° respect to the horizontal during the tests). The same features are also well identified in Fig. 2. Moreover, SEM images taken at higher magnification showed the presence of cracks and micro-cracks at the surface. Cracks are perpendicular to the direction of the flux and increase with increasing heat load from A3 to A1.

Tungsten doped with lanthanum oxide forms an alloy in which the particles are dispersed in the W matrix and easily distinguishable: their elongated structure is the result of the rolling process

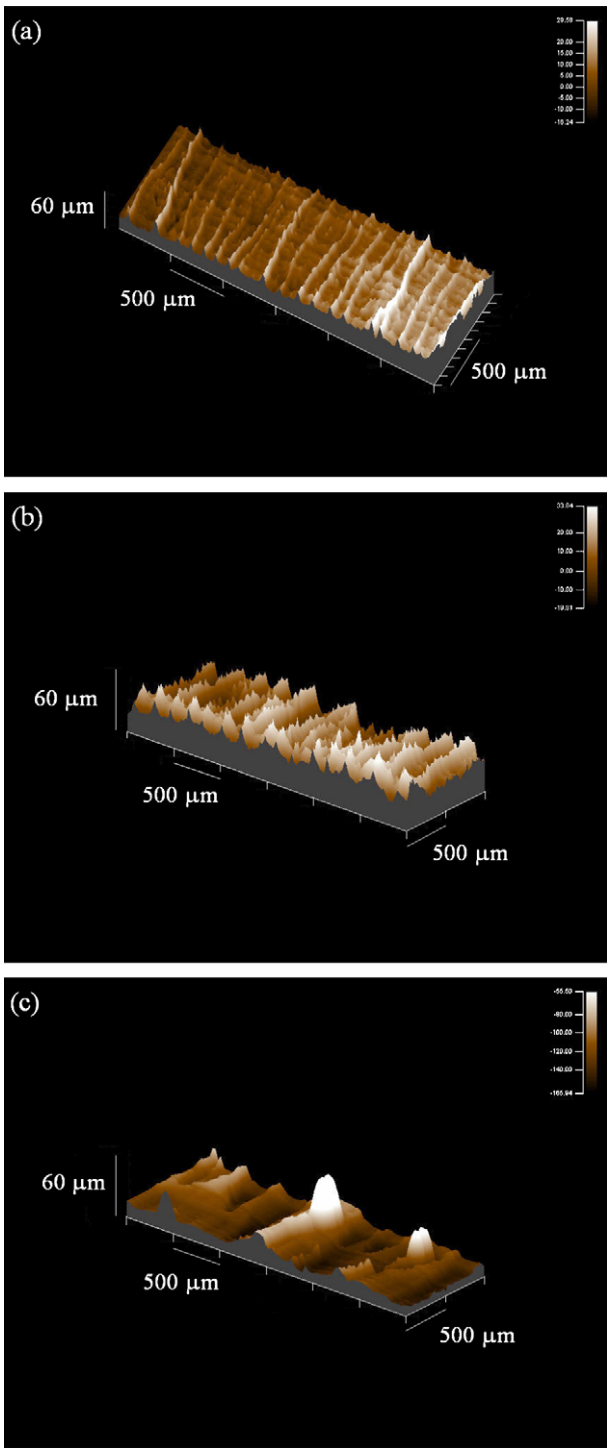

Fig. 2. 3D profile of the samples (a) A1 (b) A2 and (c) A3.

and is parallel to the rolling direction. The presence of La_2O_3 particles is detected by measuring the lanthanum MNN and NOO, the oxygen KLL, the tungsten MNN and NOO Auger spectra and by observation of the SEM images of the samples in Secondary Electrons Detection (SED) and Back-Scattered Electrons (BSE) mode in the SAM apparatus.

La_2O_3 particles are clearly visible at the surface of the virgin sample (A0) (Fig. 4), while after the thermal energy exposure particles are no longer observed on the sample surface due to the formation of the melt layer. In order to map the distribution of the

Table 1
Summary of the surface damage for three different materials exposed to the same load 1 MJ/m^2 obtained with the profilometer. Sample W3 is pure W. Its roughness was measured far away from the displaced material. CFC3 is a Carbon–Fiber–Reinforced-Carbon. For this sample too the roughness was measured far away from the eroded material. Crest and valley refer to the undulation created by the erosion. The letters indicate different regions of the samples examined.

Sample W–La_2O_3	Roughness (μm)	Height of crests (μm)	
A1	33.83	40	
A2	6.84	20	
A3	9.36	20	
Sample W3	Roughness (μm)	Depth of crack (μm)	Height displaced material (μm)
Reference	1.43	–	
D1	1.53	2	
D2	11.95	7	
D6	6.27	10	
D7	1.62	20	38.8
D8		4	30.7
Sample CFC3	Roughness (μm)	Craters	
		Base width (μm)	Depth (μm)
Blank	6.06	150	100
D1	30.88	300	90
D2	105.22	600	120
D6	113.12	600	150
D7	73.28	700	200
D8	24.15	700	100

particles inside the bulk of the samples, they have been fractured in liquid nitrogen and then analyzed: Fig. 5 shows, as an example, the presence of particles in the section of sample A3. The SAM analysis enables an unambiguous association between the morphological features observed on the surface in SEM image (Fig. 5) and: (1) the La_2O_3 particles, (2) their negative mark corresponding to particles attached to the complementary side of the fracture or to the cavity left by a particle laying there before the irradiation, as discussed in the next section. Fig. 6 shows the Auger spectra relative to a La_2O_3 particle (top), a negative mark/cavity where there are no significant traces of La (middle) and the tungsten matrix (bottom) relative to Fig. 5. The regions used for the measurement of the density of the particles are rectangular area $100 \times 40\ \mu m^2$ with the shorter side along the normal to the exposed surface. Fig. 7 shows the profiles of particle density (measured as the sum of present particles, point 1 above, and negative marks, point 2) together with the corresponding tendency curves, either for the virgin reference material A0 [12] (before thermal exposure) and for the samples A1, A2 and A3 (after thermal exposure).

4. Discussion

The 3D profiles measured by the profilometer clearly show that the thermal exposure induces an enhanced surface damage. The development of corrugations in the direction of the flux recalls the behavior of a (CFC) [13] sample rather than a W one. Moreover, it is also evident from Fig. 2 that going from sample A3 to A1 the increase of thermal load due to the plasma profile corresponds to more important melting effects, such as displacement and undulation. As a rough estimate, the thickness of the melted volume is of the order of a few hundred microns in the most irradiated sample: since the melting heat for tungsten (W) is 35.4 kJ/mol and the molar volume is 9.47×10^{-6} m^3/mol, the energy density able to melt a piece of W 300 μm thick is around 1 MJ/m^2 [14]. The clearly observed surface morphological damages and the strong structural modification of the alloy whenever the melting temperature is exceeded, indicate that there are no advantages in the use of a W–La_2O_3 armor instead of a pure W [11].

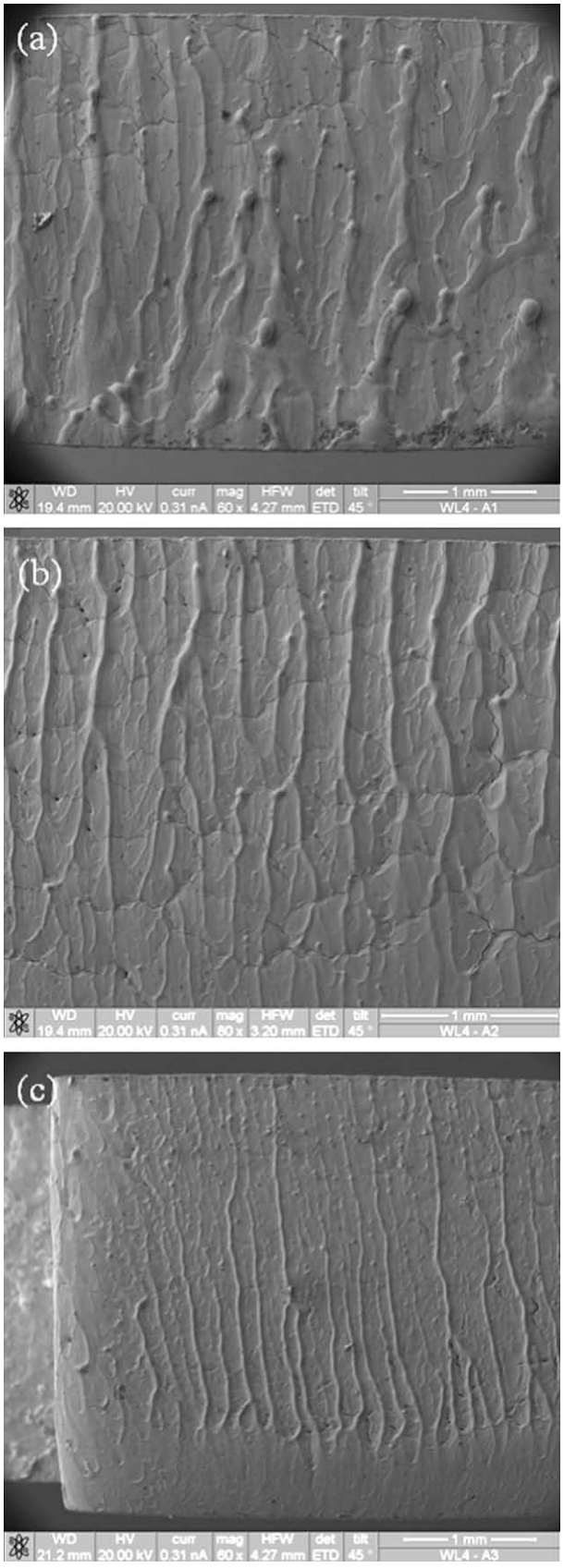

Fig. 3. SEM image at magnification 80× on the sample surface for (a) A1 (b) A2 and (c) A3.

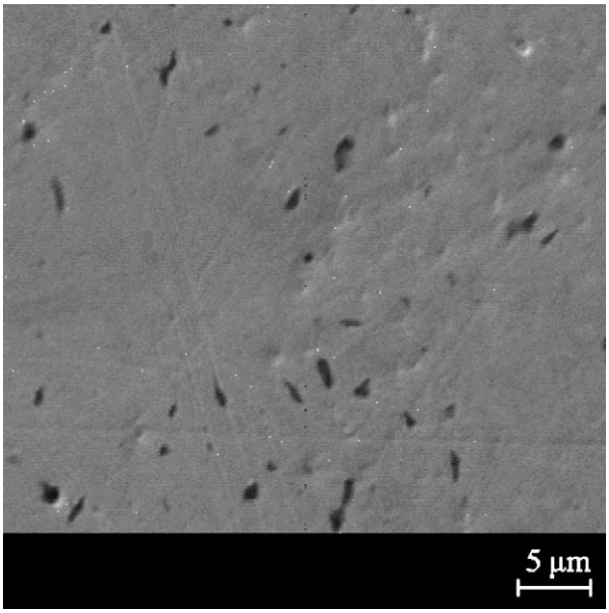

Fig. 4. SEM image at magnification 3000× at the surface of the virgin sample (A0).

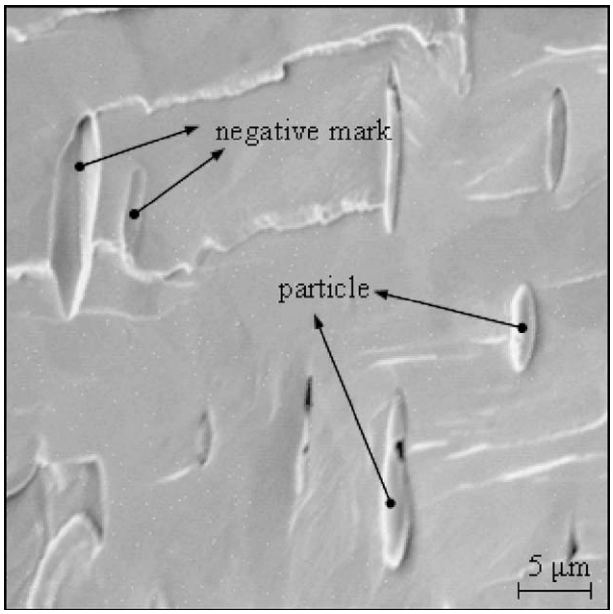

Fig. 5. SEM image at magnification 3000× in the sample section for A3.

The results from the SAM analysis show that the damage is extended further in depth into the bulk of the shielding armor, due to solid state processes activated at temperatures below the melting point. Looking at the depth profiles of the particle density, two striking features have to be pointed out for all the samples subjected to the thermal load (A1, A2 and A3): (i) there are essentially no La_2O_3 particles at the surface in a volume 20 ÷ 40 μm thick, (ii) then the density increases smoothly with depth and (iii) the rate of density variation decreases with depth leading most probably to a steady value at some point out of our field of view. The higher the thermal load delivered to a sample, the lower is the density at a given depth within the observed range. These observations further advise against the exploitation of the W–La_2O_3 as divertor material.

A detailed investigation of the mechanisms involved in this structural evolution is not the goal of this work, however we propose in a strictly tentative way a rationale to interpret our experimental results, based on the thermodynamic equilibrium and kinematic considerations at the length scale of the La_2O_3 particle size.

The melting and evaporation temperatures for bulk W are at 3422 and 5555 °C, respectively, while for bulk La_2O_3 the corresponding values are at 2315 and 4200 °C. It is possible that the La_2O_3 particles vaporize at a temperature comparable to or even lower than the melting temperature of the bulk W [15], due to the reduction of their surface energy, which is particularly convenient when the surface to volume ratio is high (as it is the case). Thus it seems reasonable that: (1) in regions far from surface where the material did not melt, the La and O could dilute in atomic or molecular form straight from the particle and disperse into the W bulk by a solid state diffusion process; (2) in the melted volume close to the surface, on top of the diffusion process, the higher mobility of the material could also allow part of the gases containing La and O to escape into the ambient [16]. Assuming a roughly homogeneous distribution of La atoms into the bulk W, the dilution following process (1) could lower the concentration of La below the sensitivity of our SAM apparatus: this could explain the absence of the La signal in the Auger spectrum measured from the substrate bulk (see Fig. 6, bottom panel).

The explanation of the lower density of particles and/or particle cavities, requires to take into account the solid state diffusion of the W atoms over the length scale of the particle size. The diffusing W atoms could fill the empty space left by the particles in the solid phase, driven by a surface energy gain [17,18] similar to that mentioned in point 1, thus lowering the particle density. In the melted region the much higher mobility of the flowing material would

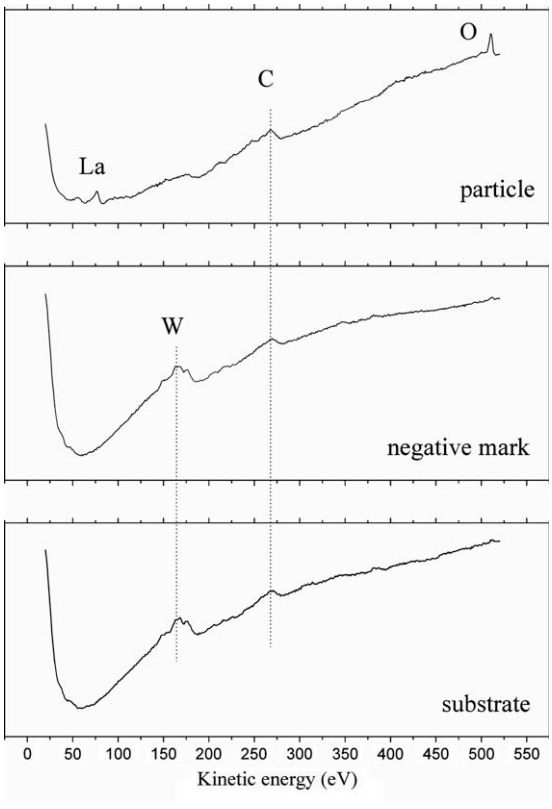

Fig. 6. Auger spectra relative to the morphological features of Fig. 4: La_2O_3 particle (top), negative mark (middle) and W matrix (bottom).

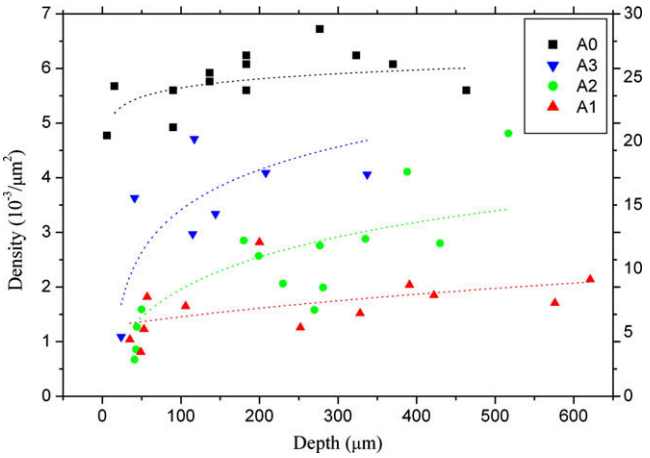

Fig. 7. Depth profile of the La_2O_3 particles density distribution and correspondent tendency curves. The density scale for the virgin material A0 is on the right side, while for the samples A1, A2 and A3 is on the left side.

greatly enhance this process and could easily justify the total absence of particles close to the surface. This mechanism is also consistent with the fact that the particle densities found in the irradiated samples (A1, A2 and A3) turn out to be much lower than the density in the A0 reference and that their values decrease monotonically with increasing the thermal load.

5. Conclusions

A W–(1%)La_2O_3 castellated armor was exposed to 100 ELM's transients at the QSPA facility. Three samples of this armor with an estimated deposited energy density of respectively 1, 0.8 and 0.6 MJ/m^2 have been analyzed with different techniques in order to study the surface damage and the bulk structural modifications. The profilometry measurements pointed out enhanced surface erosion in the direction of the plasma flux. A comparison with previous results obtained with Carbon–Fiber–Reinforced-Carbon and W samples indicates that the surface morphological modifications resemble those found for the Carbon–Fiber–Reinforced-Carbon samples rather than those for W samples. The erosion at the surface increases with the thermal load and appears (at equal load) to be larger with respect to pure W.

SEM analysis revealed the onset of melting effects, such as displacement and undulation, on the surface. Finally, the depth profiles of the La_2O_3 particle density obtained with SAM mapping on the sample sections showed a specific trend as a function of the depth and of the thermal load, for which a tentative interpretation based on thermodynamic and kinematic consideration has been proposed. All of these findings suggest that W–La_2O_3 armor shows a worse performance than a pure W one when exposed to simulated ELM's transients.

Acknowledgments

MZ and AT wish to thank M. Bestetti and A. Vicenzo (Dipartimento di Chimica e Materiali "Giulio Natta") and C. Mapelli (Dipartimento di Meccanica) of the Politecnico di Milano for useful discussions on the chemical property of ceramic dispersions in metals.

References

[1] A.A. Haasz et al., J. Nucl. Mater. 258–263 (1998) 889.
[2] F.C. Sze et al., J. Nucl. Mater. 264 (1999) 89.
[3] I. Smid et al., J. Nucl. Mater. 258–263 (1998) 160.
[4] G. Leichtfried, in: Proceeding of Second International Conference of Tungsten and Refractory Metals, Metal Powder Industries Federation, Princeton, NJ, 1994, p. 319.
[5] R.I. Jaffee, C.T. Sims, J.J. Harwood, in: Proceeding of Third Plansee-Seminar, Reutte, Austria, 1958, p. 380.
[6] G.A. Geach, J.E. Hughes, in: Proceeding of Second Plansee-Seminar, Reutte, Austria, 1955, p. 245.
[7] I. Garkusha et al., J. Nucl. Mater. 337–339 (2005) 707.
[8] ITER-EDA Final Design Report, Materials Assessment Report, 1998.
[9] A. Zhitlukhin, G. Federici, R. Giniyatulin, I. Landman, J. Linke, A. Loarte, M. Merola, V. Podkovyrov, V. Safronov, Experimental Assessment of the Effects of ELMs and Disruptions on ITER Divertor Armour Materials-IT/P3/30.
[10] A. Zhitlukhin et al., J. Nucl. Mater. 363–365 (2007) 301.
[11] F. Ghezzi, Surface Morphological Modifications of Divertor Tiles during ELM's Mode, EFDA Task TW4-TPP TARCAR, IFP Report FP0802, Milan 15/04/2008. <http://www.ifp.cnr.it/publications/2008.html#MINOR7>.
[12] Supplied by the Forschungszentrum Jülich GmbH.
[13] J.P. Bonal, C.H. Wu, D. Gosset, J. Nucl. Mater. 307–311 (2002) 100.
[14] B. Bazylev, H. Wuerz, J. Nucl. Mater. 307–311 (2002) 69.
[15] H.W. Goldstein et al., J. Phys. Chem. 65 (1961) 1400.
[16] M. Bestetti, A. Vicenzo, Private Communication.
[17] W.R. Graham et al., Phys. Rev. Lett. 222 (1973) 1407.
[18] Z.M. Stepien et al., Surf. Sci. 216 (1989) 505.